scientific reports

Check for updates

OPEN

Complex coacervation of fish gelatin and sodium alginate for clove oil microencapsulation

Evren Koç[1], Neslihan Mutlu[2]✉ & Emel Kaçar[3]

Clove oil (CO), rich in phenolic compounds such as eugenol, was encapsulated to enhance its stability and antimicrobial performance. Fish gelatin (FGe) and sodium alginate (SA) were used as wall materials for encapsulation through complex coacervation. Prior to encapsulation, turbidity and zeta potential were measured as a function of pH, and coacervate yield was calculated to determine optimal coacervation conditions. The FGe: SA ratios of 3:1–5:1 and pH values between 3 and 4 were determined as optimal ranges. These parameters, together with the wall-to-core ratio (wall: core), were used as independent variables in a Box–Behnken response surface methodology (RSM) to evaluate their effects on encapsulation efficiency (EE) and encapsulation yield (EY). The highest experimental EE and EY values obtained within the design were 91.7% and 89.5%, respectively. Microcapsules prepared under the optimized conditions exhibited a moisture content of 2.57%, hygroscopicity of 8.64%, and solubility of 65.33%. Thermogravimetric analysis (TGA) confirmed enhanced thermal stability, with decomposition shifting to higher temperatures (~ 200–350 °C). In the simulated gastrointestinal system, the microcapsules remained stable under acidic conditions and released CO gradually at higher pH. Antimicrobial assays showed comparable inhibition against *Staphylococcus aureus* and significantly higher activity against *Escherichia coli* compared to unencapsulated CO. These findings suggest that FGe–SA coacervate microcapsules are a promising delivery system for clove oil in functional food applications.

Keywords Fish gelatin, Sodium alginate, Clove oil, Complex coacervation, Encapsulation

Essential oils are aromatic, volatile plant-derived compounds widely used in medicine, cosmetics, and food preservation due to their diverse biological activities[1]. Despite their remarkable biological potential, such as antimicrobial and antioxidant activities, the practical utilization of essential oils is hindered by their volatility, poor solubility, chemical instability, sensory incompatibility, and concerns related to safety and standardization[2,3].

Clove oil (CO), obtained from the buds of Syzygium aromaticum, is rich in bioactive compounds, primarily eugenol (~ 89%), along with smaller amounts of eugenol acetate and β-caryophyllene. This composition confers strong antioxidant and antibacterial properties to CO[4,5]. However, its phenolic constituents are highly sensitive to environmental factors such as light, heat, and oxygen, leading to oxidation and degradation of active compounds[6]. Consequently, the biological efficacy of CO decreases over time, limiting its stability and practical application.

To overcome these limitations, microencapsulation has emerged as an effective strategy to protect essential oils from evaporation, oxidation, and environmental degradation while improving their stability and controlled release properties[7,8]. Among various encapsulation techniques, complex coacervation is particularly attractive due to its mild processing conditions and high encapsulation efficiency for volatile bioactive compounds such as essential oils[9]. This method is based on the electrostatic interaction of oppositely charged biopolymers, leading to the formation of a protective wall around the core material upon pH adjustment, thereby reducing sensory and safety concerns and enabling controlled release[8,9].

Fish gelatin (FGe), derived from fish-processing by-products, represents a sustainable and biocompatible alternative to bovine and porcine gelatin, which are associated with disease risks and cultural or religious restrictions. In addition, FGe has been reported to exhibit a lower environmental footprint than mammalian gelatin. However, due to its lower melting point, gel strength, and proline–hydroxyproline content, FGe shows

[1]Department of Bioengineering, Faculty of Engineering and Architecture, Kafkas University, Kars, Turkey. [2]Department of Biology, Faculty of Science and Letters, Kafkas University, Kars, Turkey. [3]Plant and Animal Production Department, Avanos Fine Arts Vocational School, Nevşehir Hacı Bektaş Veli University, Nevşehir, Turkey. ✉email: n.mutlu@kafkas.edu.tr

limited thermal and mechanical stability, which can be improved through chemical modification or blending with other polymers[10].

Sodium alginate (SA) is a biodegradable and biocompatible polysaccharide derived from brown algae and is frequently combined with FGe to improve the mechanical and barrier properties of composite systems due to its viscosity-enhancing and emulsifying characteristics[10,11]. The FGe–SA combination has also been applied in hydrogel systems, where the incorporation of copper sulfide nanoparticles enhanced antibacterial activity against S. aureus and E. coli and accelerated wound healing, demonstrating the synergistic potential of these polymers[12].

To the best of our knowledge, the FGe–SA system has not been systematically optimized for complex coacervation in the presence of an active core material such as CO. Unlike most studies in which coacervation conditions are optimized prior to core addition, this work evaluates coacervate formation and encapsulation performance in the presence of CO. Accordingly, a two-step optimization strategy was applied, first assessing the effects of the FGe: SA ratio and pH on coacervate yield, followed by optimization of encapsulation parameters using RSM. Under the optimized conditions, the physicochemical properties, release behavior, and antimicrobial activity of the resulting microcapsules were investigated.

Materials and methods

Materials

Mueller-Hinton agar was purchased from Merck (Darmstadt, Germany). FGe derived from cold-water fish skin was obtained from Sigma–Aldrich (St. Louis, MO, USA). Food-grade SA (CAS No. 9005-38-3, purity = 98%) was supplied by ZAG Kimya (Istanbul, Türkiye). CO (100% purity, obtained by steam distillation) was purchased from Arifoğlu 1944 (Istanbul, Türkiye). *E. coli* ATCC 25922 and *S. aureus* ATCC 29213 were obtained from the Laboratory of Microbiology, Department of Biology, Kafkas University.

Preparation of FGe and SA stock solutions

5% (w/v) FGe stock was prepared by allowing the FGe to hydrate in distilled water at 25 °C for 30 min and then stirring at 600 rpm on a magnetic stirrer at 50 °C for 2 h. The SA stock solution (1%, w/v) was prepared by stirring SA at room temperature on a magnetic stirrer until dissolved and then keeping it overnight at 4 °C to ensure complete hydration.

Optimization of FGe–SA complex coacervation

To confirm the optimum pH (2.0–6.0) and FGe: SA ratios (1:1–6:1) of the FGe–SA coacervate systems, the turbidity, zeta potential and coacervate yield of the formed system were determined. The total concentration of complex coacervation materials (FGe + SA) was adjusted to 0.05%, 0.1%, and 1% for turbidity, zeta potential, and coacervate yield measurements, respectively[13]. Turbidity was determined in the pH range of 2.0–6.0 by measuring absorbance at 600 nm with a Multiskan SkyHigh microplate reader (Thermo Fisher Scientific, Singapore). The zeta potentials of the prepared coacervates were measured using a Malvern Zetasizer Nano ZSP (Worcestershire, UK) to determine the colloidal stability potential of each FGe: SA ratio at pH 2.0–6.0. All measurements were performed in triplicate at 25 °C. To determine the coacervate yield, the coacervates were first adjusted to the optimum pH value (3.0) obtained from turbidity measurements to obtain maximum complex coacervation. Subsequently, centrifugation (10,000×g, 10 min) was applied to collect the formed coacervates, and the obtained coacervates were dried at 105 °C to constant weight. The coacervate yield was then calculated according to the following Eq. (1):

$$\text{Coacervate Yield } (\%) = \frac{M_{FGe+SA}}{M_{FGe} + M_{SA}} \times 100 \tag{1}$$

Here, M_{FGe+SA} is the mass after the coacervate is prepared, and M_{FGe} and M_{SA} are the amounts of FGe and SA added to the coacervate.

Optimization of microcapsules by RSM

pH and wall: core ratio have been shown as critical factors for EE (%) and EY (%) in previous studies[14–16]. The experimental conditions used in the RSM design for CO-loaded FGe–SA microcapsules (FGe–SA/COMs), including pH values (3.0, 3.5, and 4.0), FGe: SA ratios (3:1, 4:1, and 5:1), and wall: core ratios (1:1, 2:1, and 3:1), are summarized in Table 1. The total wall material concentration was fixed at 1% (w/v), a low-solids level commonly used in protein–polysaccharide complex coacervation to balance processability (viscosity/emulsification) and capsule formation[13]. Using the Box–Behnken design, 15 different experimental runs were generated, as seen in Table 1. EE (%) and EY (%) were considered as the response variables in the design, and the experimental data were fitted to a second-order polynomial model (Eq. 2) to describe their relationship with the independent variables (pH, FGe: SA ratio, and wall: core ratio).

$$\mathrm{Y} = \beta_0 + \beta_1\mathrm{A} + \beta_2\mathrm{B} + \beta_3\mathrm{C} + \beta_{11}\mathrm{A}^2 + \beta_{22}\mathrm{B}^2 + \beta_{33}\mathrm{C}^2 + \beta_{12}\mathrm{AB} + \beta_{13}\mathrm{AC} + b_{23}\mathrm{BC} \tag{2}$$

where Y represents the dependent response (EE % or EY %); β_o is the intercept; β_1, β_2, and β_3 are the linear coefficients; β_{11}, β_{22}, and β_{33} are the quadratic coefficients; and β_{12}, β_{13}, and β_{23} are the interaction coefficients. A, B, and C correspond to pH, FGe: SA ratio, and wall: core ratio, respectively.

To produce FGe–SA/COMs by complex coacervation, the method described by Djihad et al., was used with modifications[17]. FGe and SA stock solutions were prepared as described in "Preparation of FGe and SA stock

Run	Conditions (independent variables)			Response variables	
	pH	FGe: SA	Wall: core	EE (%)	EY(%)
1	3.5	4:1	2:1	74.3	66.2
2	3.0	4:1	3:1	91.7	89.5
3	4.0	5:1	2:1	80.0	71.8
4	3.5	5:1	1:1	71.7	67.2
5	3.5	3:1	3:1	67.2	59.1
6	3.5	3:1	1:1	67.5	47.0
7	3.5	5:1	3:1	91.3	88.9
8	3.5	4:1	2:1	75.2	64.2
9	4.0	4:1	3:1	72.4	71.0
10	3.0	4:1	1:1	78.8	70.1
11	3.0	5:1	2:1	82.2	72.5
12	3.0	3:1	2:1	79.8	70.9
13	3.5	4:1	2:1	73.8	68.3
14	4.0	4:1	1:1	68.1	64.9
15	4.0	3:1	2:1	54.5	42.0

Table 1. Design matrix of the Box-Behnken method and its experimental results.

solutions". Then, the essential oil was gradually dropped into the FGe solution to obtain an oil-in-water emulsion and homogenized at a constant speed (9500×g, 10 min) using an Ultra–Turrax homogenizer (DAIHAN Scientific Co., Korea). The SA solution was added to the resulting emulsion, and the mixture was stirred for an additional 15 min at 600 rpm on a magnetic stirrer. The pH was adjusted to three values (2.0, 3.0, and 4.0), where turbidity was the highest and the zeta potential was closest to zero, using 0.1 M HCl with a digital pH meter (Seven Exellence, Mettler Toledo, Switzerland). The microcapsules were collected by centrifugation at 9000×g for 20 min at 4 °C using a refrigerated centrifuge (Thermo Fisher Scientific, USA). The structural integrity of the capsules was maintained using a freeze-dryer (FDCF-12012, Operon, Gimpo, Republic of Korea). The microcapsules were frozen at − 18 °C for 24 h and then freeze-dried for 48 h. They were stored in aluminum bags at 4 °C until further analysis.

Encapsulation efficiency of microcapsules

The encapsulation efficiency (EE) of the microcapsules was determined by modifying the methodology described by Zhang et al., (2023). A capsule sample (0.5 g) was mixed with 50 mL of ethanol and gently shaken to dissolve the surface oil[18]. The solution was centrifuged (9000×g, 10 min), and the supernatant was collected to determine the free CO content by UV-Vis spectrophotometry (Multiskan SkyHigh, Thermo Fisher Scientific, Singapore) at 287 nm. To determine the total CO content, 0.5 g of the capsule sample was mixed with 50 mL of ethanol and subjected to an ultrasonic bath (Bandelin Electronic RK 255 H, Germany) at 25 °C, with a power of 160 W and a frequency of 35 kHz for 20 min, to ensure complete extraction of the oil into the solvent. The extract was filtered, and the filtrate was analyzed by UV-Vis spectrophotometry at 287 nm. Absorbance values were converted to concentrations using a calibration curve, and the EE % was calculated according to the following Eq. (3):

$$EE\ (\%) = \frac{(Total\ CO - Free\ CO)}{Total\ CO} \times 100 \tag{3}$$

where *Total CO* is the total amount of CO in the microcapsules, and *Free CO* is the amount of surface oil.

Encapsulation yield of microcapsules

The encapsulation yield (EY%) was calculated according to the method described by Liu et al.[19]. For EY determination, the ratio of the total weight of the dried microcapsules to the total weight of the initial wall and core materials was expressed as a percentage, as shown in Eq. (4)[19]:

$$EY\ (\%) = \frac{W_1}{W_0} x100 \tag{4}$$

where W_1 represents the dry mass (g) of the microcapsules after freeze-drying, whereas W_0 refers to the sum of the masses of the wall material and the oil added in the encapsulation process.

Characterization of the microcapsules

Morphology

The morphological characteristics of FG–SA/COMs were examined before freeze-drying using an optical microscope (Leica DM 500, Leica Mikrosysteme Vertrieb GmbH, Wetzlar, Germany) at 100×. After freeze-drying, the morphological characteristics were examined by Scanning electron microscopy (SEM) (Carl Zeiss

Gemini 300, Jena, Germany). The samples were fixed onto a metal stub with double-sided carbon tape, coated with a thin layer of gold, and observed at an accelerating voltage of 15 kV with magnifications ranging from 50× to 5000×.

Hygroscopicity, moisture content, and water solubility

Hygroscopicity and water solubility were determined using the methods described by Daza et al.[20]. A 2 g sample was weighed and placed in a desiccator containing a saturated Na_2SO_4 solution, providing 81% relative humidity, and kept at room temperature for 7 days. At the end of this period, the sample was reweighed. Hygroscopicity was expressed as grams of water absorbed per 100 g of solid sample. Moisture content was determined using the method of Chen et al.[21]. A 1 g microcapsule sample was dried in an oven at 105 °C until a constant weight was reached. The moisture content (%) of the microcapsules was calculated from the difference between the weight before and after drying.

For the determination of solubility, 0.5 g of sample was mixed with 50 mL of distilled water and stirred at 100 rpm on a magnetic stirrer for 30 min at room temperature (25 ± 2 °C). The mixture was then centrifuged at 9000×g for 5 min, and the supernatant was transferred to a pre-weighed porcelain capsule. It was subsequently dried in an oven at 105 °C until complete evaporation of water. Solubility was calculated and expressed as a percentage (%).

Crystallinity

The crystalline structures of the microcapsules, coacervates, and the wall and core materials, the X-ray Diffraction (XRD) patterns were obtained using an X-ray diffractometer (Bruker AXS D8 Advance, Madison, WI, USA), operated at 40 kV, 40 mA, and 1.540 Å. Spectra were recorded using CuKα radiation. Distribution patterns were obtained at 2θ angles ranging from 5° to 50° at a scanning rate of 10°/min at room temperature (25 °C)[22].

Chemical structure

The chemical structures of non-encapsulated CO, freeze-dried FGe, SA, coacervate powders, and microcapsules were evaluated by Fourier transform infrared (FTIR) spectroscopy. FTIR analysis was performed using the KBr pellet method in the range of 4000–400 cm^{-1} with a resolution of 4 cm^{-1} and 32 scans, using a Nicolet iS50 spectrometer (Thermo Fisher Scientific, USA).The FTIR spectra of the wall and core materials, coacervates, and microcapsules were obtained[14].

Thermogravimetric analysis

To evaluate the thermal stability of the non-encapsulated CO, freeze-dried coacervate powders, and microcapsules, a thermogravimetric analyzer (TA Instruments SDT-650, USA) was used. Thermal analyses were carried out in the range of 30–600 °C at a heating rate of 10 °C/min under a nitrogen atmosphere[11].

In vitro simulated gastrointestinal release

The in vitro release of encapsulated CO was evaluated based on the method described by Hosseini et al., (2013) with modifications[23]. For the simulated gastrointestinal digestion, freeze-dried FGeSA/COMs (20 mg) were dispersed in 5 mL of release medium consisting of 60% phosphate-buffered saline (PBS) and 40% ethanol, and incubated at 37 °C. The digestion process was simulated sequentially in two stages.

In the gastric phase, the medium was adjusted to pH 1.2 and the samples were incubated for 120 min, during which aliquots were withdrawn at 30, 60, 90, and 120 min. After completion of the gastric phase, the pH of the medium was adjusted to 6.8 using 1 M NaOH to simulate intestinal conditions, and the incubation was continued for an additional 180 min. During this period, aliquots were collected at 30 min intervals. At each sampling time, the suspension was centrifuged at 9000×g for 5 min at 25 °C, and a defined volume of supernatant was withdrawn for analysis and replaced with an equivalent volume of fresh medium to maintain constant volume. The concentration of released CO was measured by UV-Vis spectrophotometry at 275 nm. The cumulative release (%) of CO was calculated according to the following Eq. (5):

$$Cumulative\ release\ (\%) = \frac{M_t}{M_0} \times 100 \tag{5}$$

where M_t is the total amount of CO released at time t, and M_o is the total amount of CO initially encapsulated in the sample.

When aliquots were withdrawn and replaced with fresh medium during the release test, the total released amount (M_t) was corrected using the following Eq. (6):

$$M_t = C_t\ x\ V_t + \sum_{i=1}^{n-1} (C_i\ x\ V_s) \tag{6}$$

where C_t is the CO concentration in the release medium at time t, V_t is the total volume of the release medium (mL), C_i is the concentration of CO in each previously withdrawn sample, and V_s is the volume of each withdrawn sample (mL).

Antimicrobial properties of microcapsules

The agar well diffusion method modified from Plati & Paraskevopoulou, (2023) was used to evaluate the antibacterial efficacy of the microcapsules against *E. coli* and *S. aureus*[16]. 0.1 mL of each bacterial suspension (~1.5×10^8 CFU/mL) was inoculated onto Mueller Hinton agar plates. Wells (10 mm in diameter) were aseptically

punched into the agar using a sterile cork borer. Dry capsules containing 2.5–10.0 mg of CO were weighed in appropriate amounts and placed into the wells. The oil content (Total CO) was calculated and determined as described in Sect. 2.5. For comparison, unencapsulated CO at equivalent loads (2.5 and 10.0 mg) and oil-free FGe–SA coacervates were used.

Statistical analysis

For encapsulation optimization, statistical analyses were performed using Minitab software version 22.3 (Minitab LLC, State College, PA, USA). RSM based on a Box–Behnken design was applied, and the effects of pH, FGe: SA ratio, and wall: core ratio, as well as their 2-way interactions, on EE and EY were evaluated by ANOVA, while the optimal conditions were predicted using the Response Optimizer in Minitab.

The additional statistical analyses were performed using SPSS version 22 (IBM, Chicago, IL, USA). The Kolmogorov–Smirnov test was applied to assess the normality of the data distribution. For normally distributed groups, one-way ANOVA followed by Tukey's post hoc test was used to determine statistical differences. For non-normally distributed groups, the Kruskal–Wallis test was applied to evaluate statistical differences, and Dunnett's T3 post hoc test was used to assess pairwise differences. A p-value of < 0.05 was considered statistically significant.

Results and discussion

Optimization of FGe–SA complex coacervation conditions

Complex coacervation is a reaction driven by electrostatic interactions between oppositely charged biomolecules[24]. Since pH affects the ionization of functional groups, it plays a critical role in optimizing coacervation. Zeta potential and turbidity of the coacervates were measured at various pH levels and FGe: SA ratios (1:1–6:1, w/w) to determine the conditions promoting effective complex coacervation. Both turbidity and zeta potential results are presented in Fig. 1A,B. The coacervation yields obtained at the pH values corresponding to maximum turbidity for different FGe: SA ratios are also shown in Fig. 1C.

Fish gelatin has been reported to exhibit an isoelectric point (pI) around pH 7.6[25], at which the zeta potential reaches zero. Below this value, gelatin molecules carry positive charges due to protonated amino groups, while above the pI they become negatively charged owing to ionized carboxyl groups. In contrast, SA remains negatively charged over a wide pH range[21,26,27], although its zeta potential approaches neutrality at very low pH values (< 2.0) due to the protonation of carboxyl groups (pKa ~ 3.5)[27], thereby reducing the negative charges along the polymeric chain[26]. Therefore, electrostatic attraction between positively charged FGe and negatively charged SA is favored in the acidic region below the pI of FGe, which explains the effective coacervation observed in the pH 2.0–4.0 range (Fig. 1A). As shown in Fig. 1B, when different FGe: SA ratios were examined in the FGe and SA systems, it was observed that the pH ranges at which the zeta potential approached zero varied for each formulation. In our study, at higher FGe ratios (4:1, 5:1, 6:1), the zeta potential shifted to more

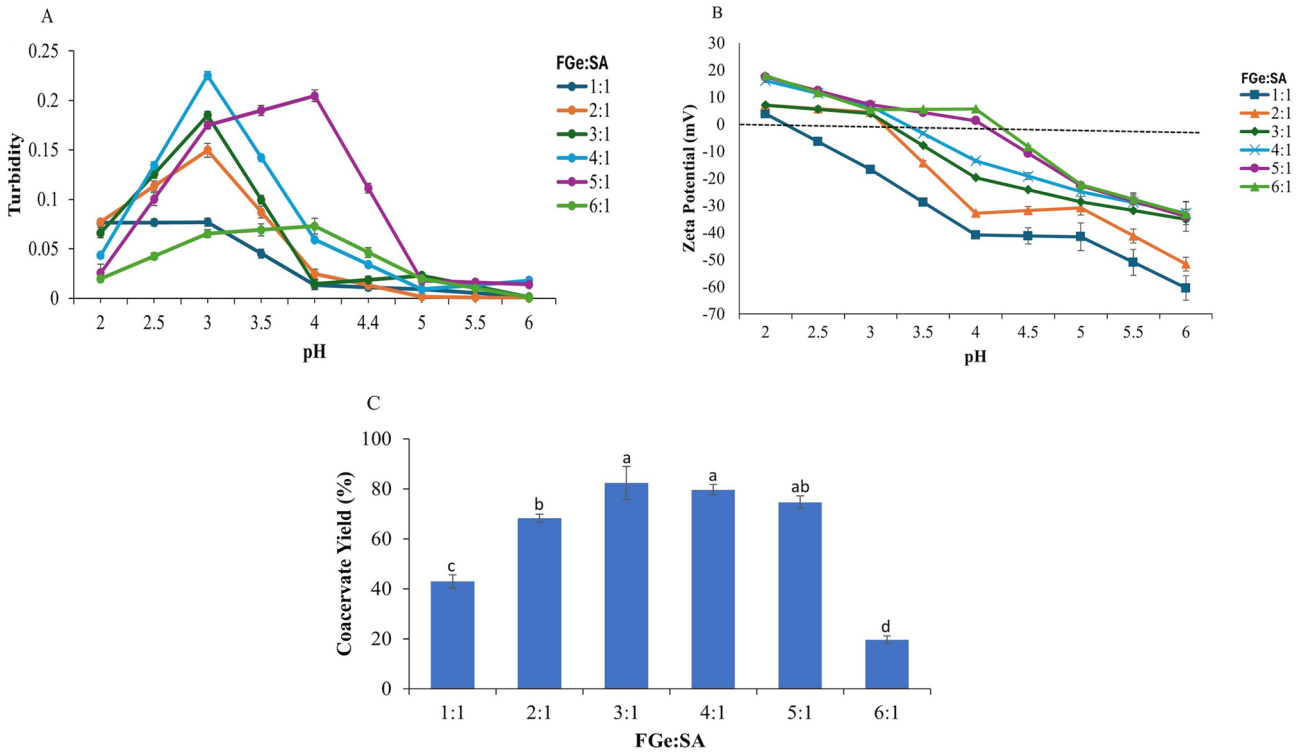


Fig. 1. Effect of pH and FGe: SA ratio on the turbidity (**A**) and zeta potential (**B**) of FGe-SA systems, and coacervate yield of FGe: SA systems.

positive values and charge neutralization occurred at higher pH values. In contrast, at lower FGe ratios (1:1 and 2:1), the zeta potential rapidly shifted to negative values due to the dominance of the negative charge of SA, and the neutralization range was reduced. These findings are consistent with previous studies showing that an increase in protein content delays phase separation, whereas lower ratios make the negative charges in the system dominant[13,28,29]. Moreover, the agreement with turbidity measurements highlights the close relationship between pH, charge neutralization, and phase separation behavior.

The pH values corresponding to charge neutralization indicate the points where the charges of the two oppositely charged polymers neutralize each other. Charge neutralization represents the state where electrostatic attraction is strongest, providing the most favorable conditions for complex coacervation. This effect is explained by the fact that these pH ranges lie substantially below the isoelectric point of gelatin (pI ~ 7.6), resulting in FGe acquiring a net positive charge while SA remains negatively charged[30]. As shown in Fig. 1B, the pH ranges where the zeta potential approached zero were consistent with turbidity and coacervation yield; therefore, pH 3.0, 3.5, and 4.0 were included as independent variables for encapsulation optimization. According to turbidity results, the coacervate yield was calculated at pH 3.0, which was identified as the most efficient pH value. Similarly, although turbidity measurements varied across FGe: SA ratios, the 3:1, 4:1, and 5:1 formulations consistently corresponded to the highest coacervation yields (Fig. 1C) and were thus also considered as independent variables. These selected factors were incorporated into the Box–Behnken design within the scope of RSM to optimize encapsulation conditions.

Optimization of microcapsules by RSM

The experimental data for EE (%) and EY (%) were fitted to second-order polynomial regression models. These equations describe the relationship between the response variables (EE% and EY%) and the independent factors (pH, FGe: SA ratio, and wall: core ratio), and are presented as follows (Eqs. 7 and 8):

$$\begin{aligned}\mathbf{EE}\,(\%) \quad &= 311.0 - 94.2\mathrm{pH} - 28.82\mathrm{FGe:SA} - 7.52\mathrm{Wall:core} \\ &\quad +6.03\mathrm{pH}*\mathrm{pH} - 1.817\mathrm{FGe:SA}*\mathrm{FGe:SA} \\ &\quad +1.808\mathrm{Wall:core}*\mathrm{Wall:core} + 11.550\mathrm{pH}*\mathrm{FGe:SA} \\ &\quad -4.300\mathrm{pH}*\mathrm{Wall:core} + 4.975\mathrm{FGe:SA}*\mathrm{Wall:core}\end{aligned} \tag{7}$$

$$\begin{aligned}\mathbf{EY}\,(\%) \quad &= 319 - 145.6\mathrm{pH} - 3.0\mathrm{FGe:SA} + 3.3\mathrm{Wall:core} \\ &\quad +12.73\mathrm{pH}*\mathrm{pH} - 5.12\mathrm{FGe:SA}*\mathrm{FGe:SA} \\ &\quad +4.46\mathrm{Wall:core}*\mathrm{Wall:core} + 14.10\mathrm{pH}*\mathrm{FGe:SA} \\ &\quad -6.65\mathrm{pH}*\mathrm{Wall:core} + 2.38\mathrm{FGe:SA}*\mathrm{Wall:core}\end{aligned} \tag{8}$$

The ANOVA results (Table 2) revealed that both models were statistically significant ($p < 0.01$). The EE model demonstrated strong model fit and predictive capability with $R^2 = 99.81\%$, Adjusted $R^2 = 99.48\%$, and Predicted $R^2 = 98.11\%$. In contrast, although the EY model was significant ($R^2 = 97.02\%$, Adjusted $R^2 = 91.66\%$), it exhibited a lower predictive power (Predicted $R^2 = 57.63\%$). The lack-of-fit values were found to be non-significant ($p > 0.05$) for both EE and EY models, indicating that the models adequately fitted the experimental data.

	EE(%)						EY(%)					
Source	**Sum of squares**	**df**	**Mean squares**	**F-value**	***p*-value**	**Sig.**	**SS**	**DF**	**MS**	**F-value**	***p*-value**	**Sig.**
Model	1260.29	9	140.033	296.78	0.000	***	2112.13	9	234.681	18.09	0.003	**
Linear	974.62	3	324.872	688.53	0.000	***	1623.47	3	541.158	41.71	0.001	**
pH	413.28	1	413.281	875.91	0.000	***	355.11	1	355.111	27.37	0.003	**
FGe: SA	394.81	1	394.805	836.75	0.000	***	830.28	1	830.281	63.99	0.000	***
Wall: core	166.53	1	166.531	352.95	0.000	***	438.08	1	438.080	33.76	0.002	**
Square	34.78	3	11.594	24.57	0.002	**	223.06	3	74.354	5.73	0.045	*
pH^2	8.40	1	8.400	17.80	0.008	**	37.42	1	37.416	2.88	0.150	NS
$(FGe: SA)^2$	12.19	1	12.186	25.83	0.004	**	96.67	1	96.666	7.45	0.041	*
$(Wall: core)^2$	12.07	1	12.074	25.59	0.004	**	73.39	1	73.391	5.66	0.063	NS
2-Way Interactions	250.89	3	83.632	177.25	0.000		265.60	3	88.532	6.82	0.032	*
pH × FGe: SA	133.40	1	133.402	282.73	0.000	***	198.81	1	198.810	15.32	0.011	**
pH × Wall: core	18.49	1	18.490	39.19	0.002	**	44.22	1	44.223	3.41	0.124	NS
FGe: SA × Wall: core	99.00	1	99.002	209.83	0.000	***	22.56	1	22.563	1.74	0.244	NS
Lack-of-Fit	1.35	3	0.451	0.90	0.566	NS	56.47	3	18.823	4.48	0.188	NS
Pure Error	1.01	2	0.503				8.41	2	4.203			
Error	2.36	5	0.472				64.87	5	12.975			
Total	1262.65	14					2177.00	14				
Model sum.	S = 0.6869, $R^2 = 99.81\%$, Adj $R^2 = 99.48\%$, Pred $R^2 = 98.11\%$						S = 3.6021, $R^2 = 97.02\%$, Adj $R^2 = 91.66\%$, Pred $R^2 = 57.63\%$					

Table 2. Analysis of variance (ANOVA) of the quadratic polynomial models for EE (%) and EY (%). Significance codes: $^*p < 0.05$; $^{**}p < 0.01$; $^{***}p < 0.001$; NS, not significant.

All variables had a statistically significant effect on EE (model $p < 0.001$). Among the individual factors, pH, FGe: SA ratio, and wall: core ratio each showed highly significant contributions ($p < 0.001$). The quadratic terms of these variables (pH^2, $(FGe: SA)^2$, $(Wall: core)^2$; $p < 0.01$) and their two-way interactions (pH × FGe: SA, FGe: SA × Wall: core, pH × Wall: core; $p \leq 0.01$) were also significant, indicating that EE was affected by both nonlinear effects and factor interactions. For EY, the order of importance differed. The FGe: SA ratio ($F = 63.99$, $p < 0.001$) was the strongest contributor, followed by the wall: core ratio ($F = 33.76$, $p = 0.002$) and pH ($F = 27.37$, $p = 0.003$). These results demonstrate that while all three factors significantly influenced yield, their relative contributions varied, with FGe: SA being the dominant determinant.

For EE, pH was the key determinant. As seen in Fig. 2a,a', EE was highest under acidic conditions but decreased as values approached neutrality, reflecting a non-linear trend. Similar patterns have been reported previously, showing that EE initially improves and then declines with changing pH[31]. This highlights the crucial role of maintaining low pH to ensure electrostatic interactions and effective complex formation. The second most important factor for EE was the FGe: SA ratio. Results showed a curved response (Fig. 2c,c'), with efficiency increasing at moderate ratios but declining at extreme values. This behavior can be explained by the electrostatic interactions between positively charged gelatin and negatively charged sodium alginate. At balanced ratios, sufficient oppositely charged groups interact to form stable coacervates, whereas excess protein or polysaccharide leads to charge imbalance, weakens electrostatic attraction, and reduces encapsulation efficiency. Wall: core ratio also influenced EE, as illustrated in Fig. 2b,b′. This factor, although less influential than pH and FGe: SA, also contributed significantly to EE. Increasing this ratio generally enhanced encapsulation efficiency up to a certain point. Previous studies confirm this trend: microcapsules prepared with pea protein isolate and sugar beet pectin showed an increase in EE from 1:1 to 4:1 ratios[32], while Kaushik et al., (2016) reported an improvement from 73% to 87% in flaxseed protein–flaxseed gum systems as the ratio increased from 2:1 to 4:1[33]. These observations align with the present findings, where higher wall: core ratios improved efficiency until excessive polymer concentrations impaired emulsification and polymer–polymer interactions[34,35].

For EY, the FGe: SA ratio was the most critical factor. Yield increased as this ratio rose but further increases reduced stability (Fig. 3c,c′), reflecting an imbalance in electrostatic charges. This trend is consistent with earlier reports showing that excessive protein-to-polysaccharide ratios reduce coacervate stability[36,37]. The wall: core ratio was the second most influential factor for EY. Although the trend was less pronounced than for EE, increasing the ratio moderately improved yield, supporting the role of sufficient wall material in stabilizing coacervates (Fig. 3b,b′,c,c′). pH had the smallest contribution to EY. While changes in pH influenced yield to some extent, the effect was limited compared with the other two variables (Fig. 3a,a′).

Interaction effects were also noteworthy. For EE, combinations of pH with FGe: SA and of FGe: SA with wall: core ratio produced strong synergistic responses (Fig. 2a,a′,c,c′), while the pH × wall: core effect was weaker but still significant (Fig. 2b,b′). In particular, the combination of low pH and high FGe: SA yielded the best outcomes, as gelatin retained enough positive charge to interact with sodium alginate even as pH increased (Fig. 2a,a′). For EY, the only meaningful interaction was between pH and FGe: SA, which again emphasized the importance of electrostatic balance for stable coacervate formation (Fig. 3a,a′).

The optimization analysis revealed that pH, FGe: SA ratio, and wall: core ratio were critical determinants for maximizing EE and EY. The response optimizer identified the optimum conditions at pH 3.0, FGe: SA ratio of 5:1, and wall: core ratio of 3:1. Under these settings, the model predicted values of 96.06% for EE and 91.66% for EY.

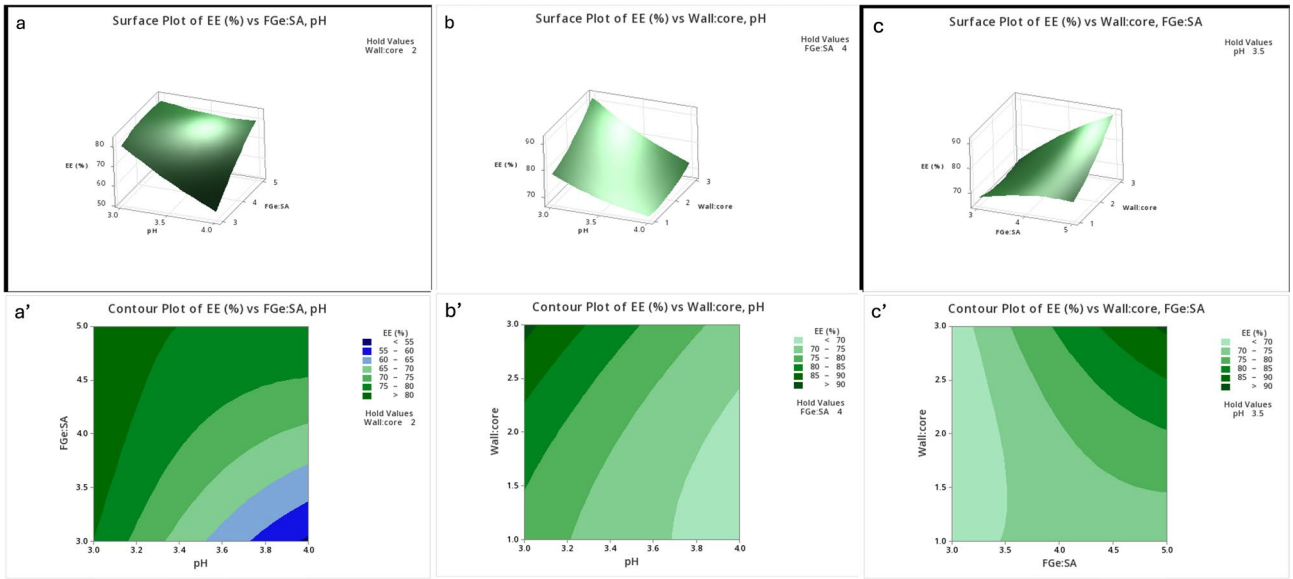


Fig. 2. Response surface (**a**–**c**) and contour plots (**a′**–**c′**) showing the effect of pH, FGe: SA ratio, and wall: core ratio on the EE (%) of microcapsules.

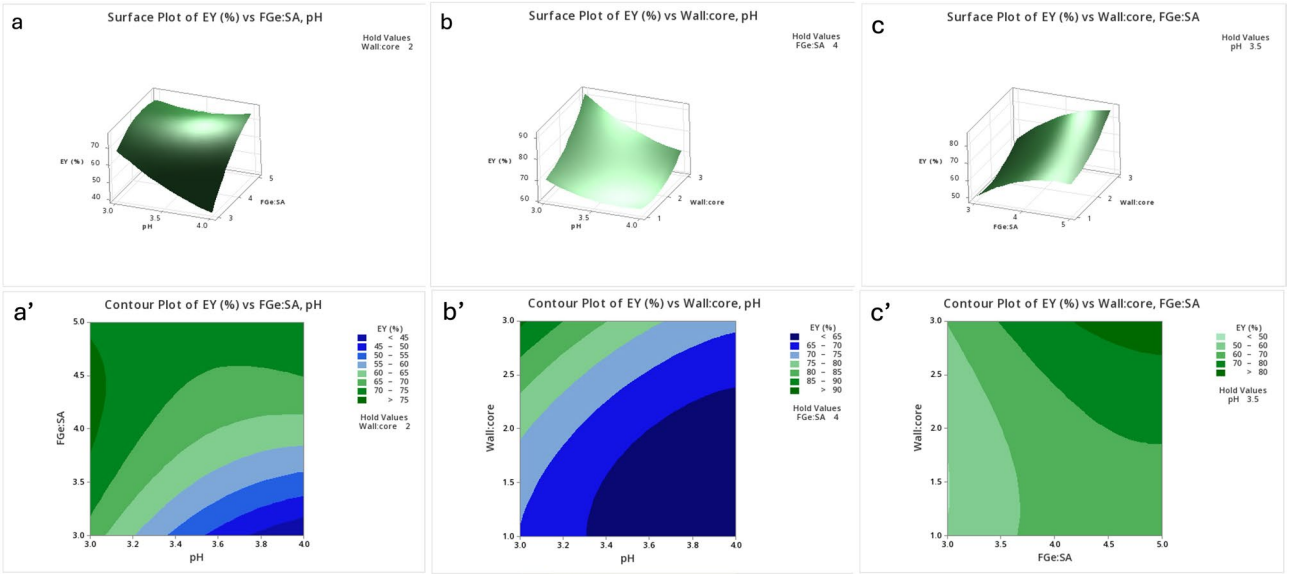


Fig. 3. Response surface (**a**–**c**) and contour plots (**a′**–**c′**) showing the effect of pH, FGe: SA ratio, and wall: core ratio on the EY(%) of microcapsules.

Although the optimum pH obtained from the coacervation optimization study was 4.0 for the 5:1 system and 3.0 for the other ratios ("Optimization of FGe–SAcomplex coacervation conditions"), the encapsulation experiments indicated that pH 3.0 provided the highest efficiency overall. The difference between the optimum pH values obtained during coacervation optimization and encapsulation can be explained by changes in electrostatic and interfacial interactions caused by the introduction of the oil phase. In empty coacervates, complex formation is mainly governed by electrostatic attraction between oppositely charged biopolymers, and the optimum pH reflects their charge balance. During encapsulation, however, protein adsorption at the oil–water interface and partial shielding or redistribution of charged groups modify the effective charge density and interaction strength between the wall materials. In addition, variations in the wall: core ratio further influence this balance by altering the availability of charged sites. As a result, the pH at which maximum coacervate stability and encapsulation efficiency are achieved may differ from that of empty coacervates.

Characterization of microcapsules

Microcapsules were prepared under the optimal conditions determined by the response optimizer of the RSM model, as described in "Optimization of microcapsules by RSM", and were subsequently used for characterization.

Morphology

Optical microscopy was used to observe the liquid coacervates and microcapsules, and SEM was applied after freeze-drying (Fig. 4).

SEM analysis revealed that the coacervates exhibited an irregular and porous morphology. Numerous pores and fragile regions were observed on the surface, while particle sizes appeared relatively uniform. Such a porous and friable structure is typically associated with the lyophilization process, during which the fluid is frozen and water in the form of ice crystals is removed by sublimation, leaving voids within the matrix[38]. Similar morphologies of coacervates and other freeze-dried systems have been described in the literature, often resembling broken-glass or flake-like structures, which are mainly attributed to the formation of ice crystals during freezing and the subsequent grinding step after freeze-drying[39,40]. These findings indicate that the observed morphology of the coacervates is consistent with previous reports. SEM images of the microcapsules showed irregular shapes with a more compact and dense structure compared to coacervates. No obvious cracks or holes were detected on the surface, suggesting that the core material was still well entrapped within the wall matrix after freeze-drying and effectively protected against environmental factors. In some regions, wrinkled and uneven surfaces were observed. Such morphology is a typical feature of freeze-dried products[41]. Moreover, the wrinkled surface structure has been reported to reduce oxygen penetration into the microcapsule matrix, thereby limiting oxidation of the encapsulated compounds and improving stability[42]. This suggests that the obtained microcapsules can provide protection for bioactive substances.

Hygroscopicity, moisture content, and water solubility

Hygroscopicity in powders can induce agglomeration and lipid oxidation, which is attributed to the interaction of water molecules with available hydroxyl groups in the amorphous and crystalline regions of carbohydrate carriers[43]. The microencapsulation by complex coacervation could decrease the hygroscopicity of microcapsules[44]. However, the extent of this reduction may vary depending on the type and composition of the carrier materials used[45]. The hygroscopicity of the microcapsules prepared under the optimal conditions was 8.64 ± 1.19%.

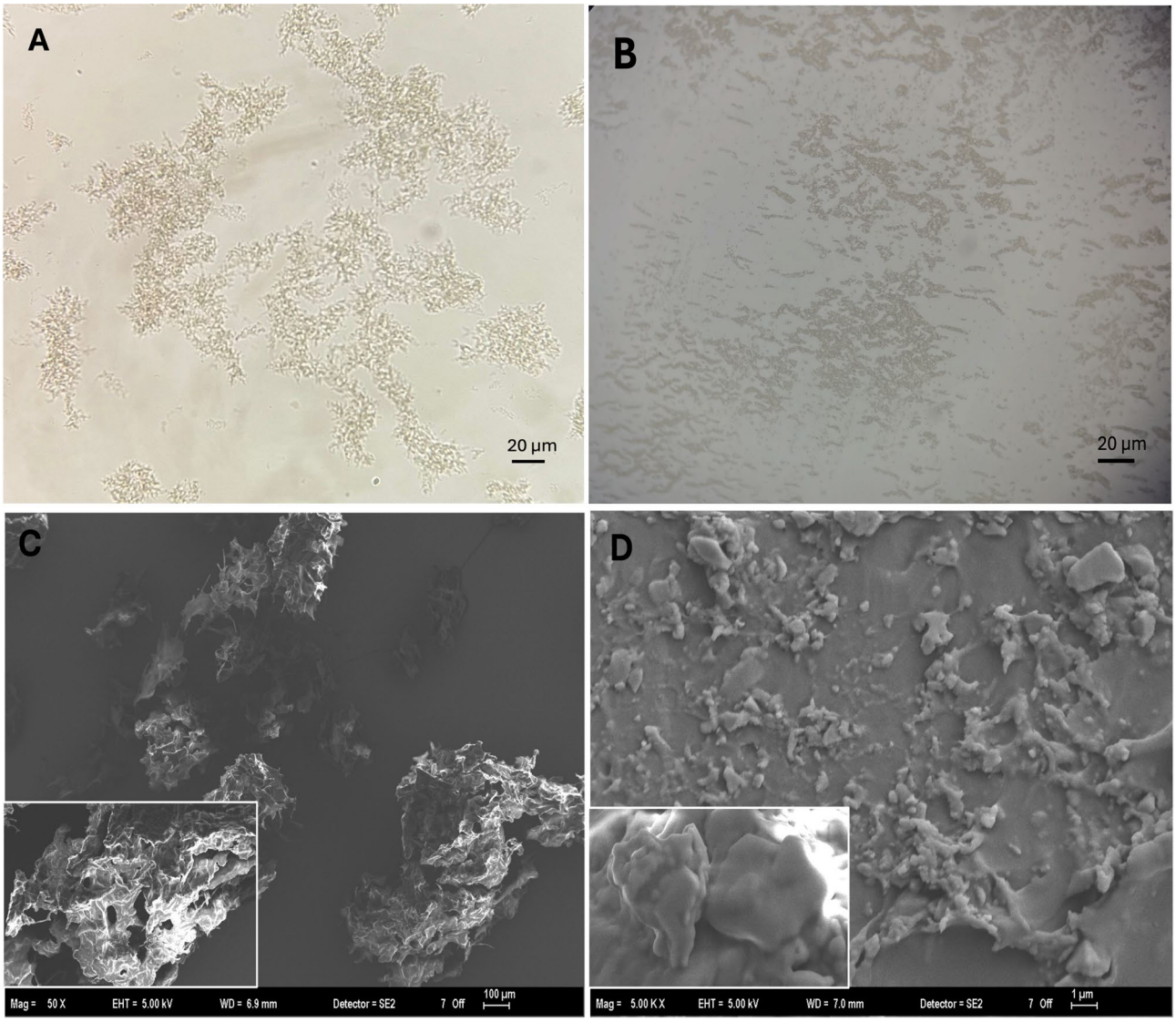


Fig. 4. Optical microscopic images of liquid coacervates (**A**) and microcapsules (**B**) at ×100; SEM images of freeze-dried coacervates (**C**) at ×50 and microcapsules (**D**) at ×5,000 magnification.

According to Tavares and Zapata Noreña (2019), powders with hygroscopicity values above 15 g/100 g are considered hygroscopic[46], while Nurhad et al., (2012) classified those exceeding 20% as highly hygroscopic[47]. In this study, the obtained value (8.64 ± 1.19%) was below these limits, indicating low hygroscopicity and suggesting good storage stability of the microcapsules.

The quality and storage stability of dried microcapsules are strongly affected by factors such as the dryer design, processing parameters, feed composition, and environmental conditions including moisture content, water activity, and temperature[48,49]. These characteristics may also vary depending on the type and concentration of the gelatin used, as both moisture-related properties and water activity were reported to be influenced by gelatin type[50]. In the food industry, Klinkesorn et al., (2006) reported that a moisture content of 3–4% is generally considered optimal for maintaining the shelf stability of dried powders[51]. Moisture levels below 5% reduce microbial spoilage and enhance the shelf-life of dried powders[52]. The moisture content of the microcapsules obtained in this study was 2.57 ± 0.34%, indicating that they possessed an optimal moisture level for extended shelf-life stability.

Solubility is an important functional property that influences the dissolution behavior of powders and their applicability as ingredients or additives in food formulations[53]. The solubility of microcapsules is strongly influenced by particle size, as smaller particles tend to exhibit lower solubility due to their higher surface energy and tendency to aggregate[54]. The water solubility of the microcapsules prepared under the optimal conditions was determined to be 65.33 ± 2.26%. Fish gelatin-based materials generally exhibit high solubility due to the hydrophilic nature of gelatin and the presence of polar amino acid residues. Similar behavior was reported for fish gelatin films, which showed a solubility of approximately 64%[55]. Although high solubility is generally desirable for the use of microcapsules as additives in food formulations, some studies have attributed low solubility to the

complex coacervation method, which produces water-insoluble particles due to strong electrostatic interactions between the materials, allowing a gradual and controlled release of the core in aqueous media[40].

Crystallinity

XRD analysis was used to evaluate the crystalline structure of the microcapsules. The diffraction peak pattern reflects the structural order of the material, where broad peaks indicate amorphous regions and sharp peaks indicate crystalline structures. The XRD patterns of the samples are presented in Fig. 5A. FGe shows two main diffraction peaks at around 2θ = 7–9° and 18–21°, corresponding to the triple-helix structure and the left-handed helical structure associated with the amorphous regions of the gelatin matrix, respectively[56]. The broad semi-crystalline peaks observed at approximately 2θ = 13.53° and 21.86° are characteristic of polysaccharide structures in SA, which is consistent with previously reported findings[57]. The disappearance of the characteristic SA peaks around 2θ ~ 13° in the coacervate pattern can be attributed to strong electrostatic and hydrogen-bonding interactions between the carboxyl groups of alginate and the amino groups of gelatin, which disrupt the ordered arrangement of alginate chains and lead to the formation of an amorphous structure. In both the coacervate and microcapsules, the coexistence of FGe and SA resulted in a more amorphous structure, as evidenced by the reduction or disappearance of the characteristic SA peaks. This behavior can be attributed to the partial disruption of hydrogen bonding between the two polymers, leading to decreased crystallinity in the complex matrix.

The XRD pattern of the microcapsules exhibited diffraction peaks corresponding to the wall materials, while the peak observed at 2θ = 20.96° in the coacervate shifted to 22.65° and became narrower, indicating structural rearrangements associated with the encapsulation of the oil within the polymer matrix. Compared with the pure wall materials, the diffraction peaks in the microcapsules became weaker and smoother, suggesting interactions between the oil and the polymer matrix. These non-covalent interactions may have disrupted the crystalline arrangement, resulting in increased amorphous structure, consistent with previous findings[58].

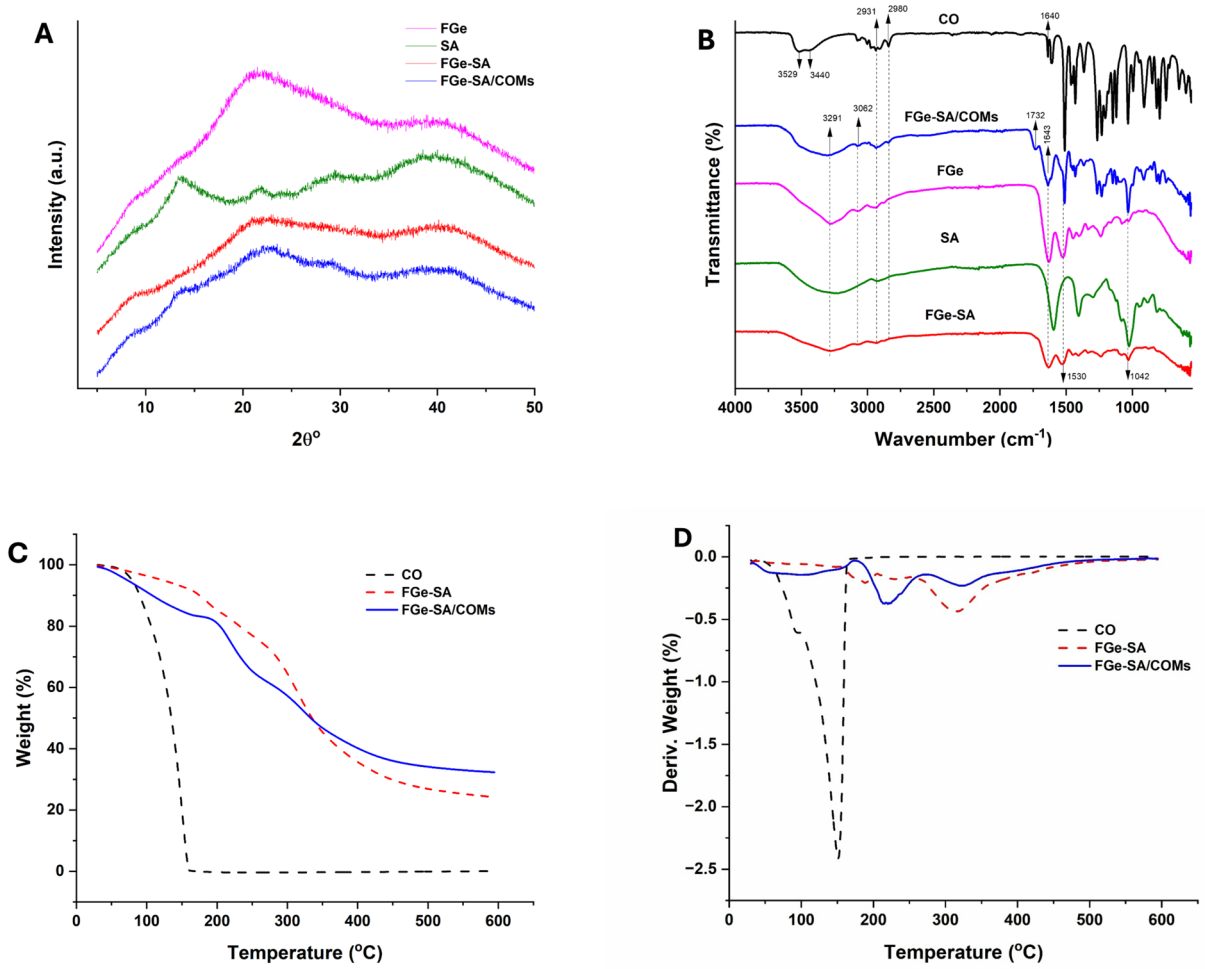


Fig. 5. XRD (**A**), FTIR (**B**), TGA (**C**), and DTG (**D**) analyses of CO, FGe, SA, FGe–SA complex, and FGe–SA/COMs.

Chemical structure

The FTIR spectra, presented in Fig. 5B, were used to identify the functional groups and assess possible interactions between the wall materials and the encapsulated oil. In the CO spectrum, absorption bands at 3529 cm^{-1} and 3440 cm^{-1} correspond to the O–H stretching vibrations of free and hydrogen-bonded hydroxyl groups, respectively[59].

The FTIR spectra of FGe and SA exhibited characteristic absorption bands associated with their functional groups. The broad band at 3291 cm^{-1} in FGe is associated with O–H and N–H stretching (amide A), indicating the presence of hydrogen bonding among gelatin molecules. The amide B band appeared at 3062 cm^{-1}, attributed to asymmetric stretching of C–H and $-NH_3^+$ groups in peptide fragments. In all spectra, absorption bands at 1931 cm^{-1} were observed, corresponding to the C–H stretching vibrations of aliphatic groups, characteristic of both the wall materials and the encapsulated oil[11]. The amide I (1643 cm^{-1}), amide II (1530 cm^{-1}), and amide III (1237 cm^{-1}) bands corresponded to C=O stretching, N–H bending/C–N stretching, and in-plane C–N/N–H vibrations, confirming the protein backbone of gelatin. In the SA spectrum, a distinct absorption band around 1042 cm^{-1} was related to C–O stretching of hydroxyl groups in the polysaccharide backbone, characteristic of alginate[60,61]. In the spectrum of the coacervate, characteristic peaks of both FGe and SA were present, though with decreased intensity and slight shifts, suggesting electrostatic and hydrogen-bonding interactions between the two polymers during complex formation. Furthermore, absorption bands at 2980 cm^{-1} and 1640 cm^{-1} were detected in both the CO and microcapsule spectra but were absent in the spectra of the individual wall materials. The band near 2980 cm^{-1} corresponds to the C–H stretching of aliphatic chains, while the one at 1640 cm^{-1} is attributed to the C=O stretching of ester or carbonyl groups in the oil[62]. The presence of these oil-specific peaks in the microcapsule spectrum indicates the incorporation of the oil into the wall material. Additionally, the characteristic C=O stretching band of the oil observed at 1640 cm^{-1} shifted to approximately 1732 cm^{-1} in the microcapsule spectrum, suggesting possible interactions between the oil and the wall material. Similar spectral shifts have been reported for microencapsulated oils, indicating the incorporation of the oil into the capsule matrix[63].

Thermal properties

The TGA and derivative thermogravimetry (DTG) curves of the samples are presented in Fig. 5C,D. Between 100 and 600 °C, the samples exhibited distinct thermal behaviors. CO showed a sharp weight loss between 100 and 200 °C, corresponding to the evaporation of volatile constituents, after which almost no residue remained. This finding indicates that the oil is thermally unstable, which is consistent with previous reports for essential oils and other plant-derived volatiles[14,64].

In contrast, the FGe–SA coacervate exhibited a gradual two-step degradation pattern: a mass loss up to approximately 200 °C associated with the removal of bound water and partial polymer decomposition, followed by a major degradation between 250 and 400 °C corresponding to the breakdown of protein and polysaccharide structures.

The FGe–SA/COMs microcapsules demonstrated an improved thermal stability compared with the CO and FGe–SA coacervate. The first mass-loss stage, observed between roughly 30 and 220 °C, can be attributed to the evaporation of residual moisture and the partial volatilization of surface or weakly bound oil fractions[65]. The second stage, occurring between about 250 and 380 °C, reflects the thermal decomposition of the gelatin–alginate wall matrix and the release or degradation of the encapsulated oil[66]. The onset of decomposition shifted to higher temperatures (~200–350 °C), indicating that the wall materials effectively protected the encapsulated oil from early volatilization and thermal degradation. This enhanced thermal stability can also be attributed to the more compact structure of the microcapsules observed in SEM images and their relatively lower moisture content, both of which likely contributed to the formation of a denser and more thermally stable polymeric matrix.

In vitro simulated gastrointestinal release

The cumulative release profile of CO from FGe–SA/COMs under simulated gastrointestinal conditions is presented in Fig. 6. During the gastric phase (pH 1.2, 0–120 min), the CO release was slow and limited, reaching around 10–15% of the total encapsulated amount. The limited release observed under gastric conditions could be attributed to several factors related to the physicochemical properties of the wall materials, including their cross-linking density, polymer–polymer interactions, and pH-dependent electrostatic behavior[67]. At low pH, protonation of gelatin and the resulting electrostatic attraction with alginate may have contributed to the formation of a compact coacervate structure, restricting oil diffusion. This behavior suggests that the microcapsules maintained their structural integrity in the acidic environment, effectively restricting oil diffusion. The limited release can be mainly attributed to the high degree of electrostatic attraction between the positively charged amino groups of gelatin and the negatively charged carboxyl groups of sodium alginate, which creates a dense and compact coacervate network. Such a structure reduces porosity and hinders the penetration of the dissolution medium, thereby slowing down the diffusion of the encapsulated oil. This interpretation is also supported by the zeta potential results, which showed higher positive surface charges at lower pH values, indicating stronger electrostatic interactions between gelatin and alginate and consequently a more stable coacervate structure under acidic conditions. These results are consistent with previous reports[68,69] which indicated that the low release in the gastric phase and the gradual increase in the intestinal phase were mainly attributed to the protective effect and low digestibility of the wall materials. When the pH was shifted to 6.8 to simulate the intestinal environment (120–300 min), the release rate increased markedly, resulting in a cumulative release of approximately 50% at the end of the digestion period. This enhancement can be explained by the changes in the electrostatic balance of the wall materials as the pH approaches the isoelectric point of gelatin (~7.6). At higher pH values, the positive charge on gelatin molecules decreases, leading to

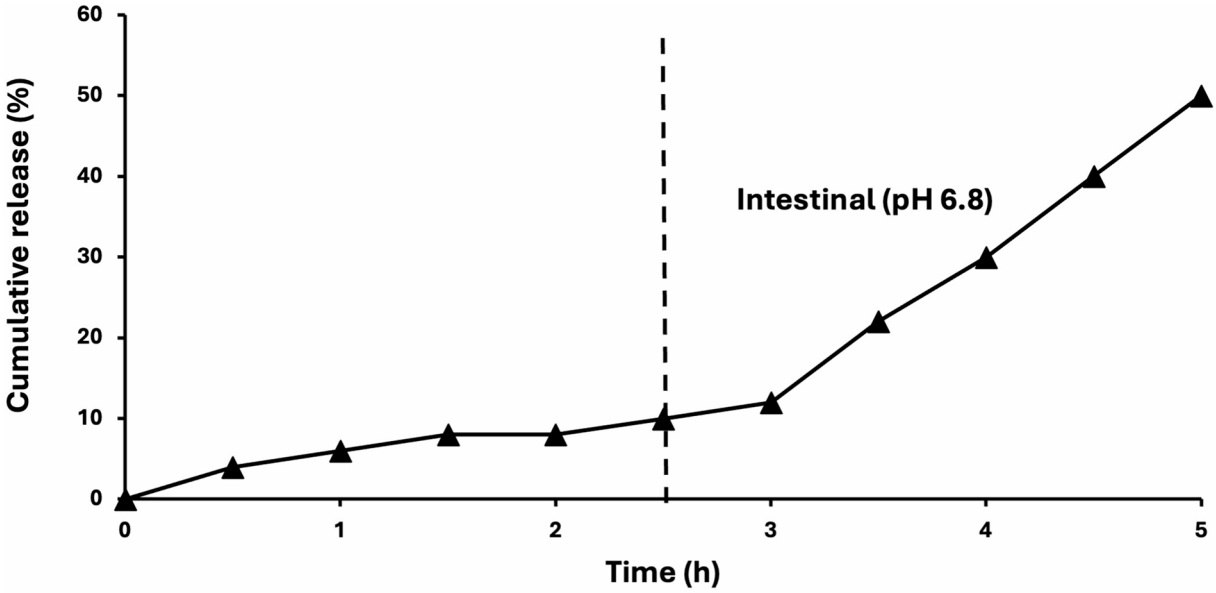


Fig. 6. Cumulative release of CO from microcapsules under simulated gastrointestinal conditions.

Bacterium	Sample type	Zone diameter (mm)		
		2.5 mg/well	5 mg/well	10 mg/well
E. coli	Unencapsulated oil	$37.07 \pm 0.35^{B,b}$	$39.90 \pm 1.15^{B,a}$	$40.92 \pm 0.95^{B,a}$
	Microcapsules	$37.00 \pm 1.52^{B,b}$	$42.42 \pm 0.83^{A,a}$	$42.53 \pm 1.16^{A,ab}$
S. aureus	Unencapsulated oil	$42.43 \pm 0.39^{A,a}$	$43.27 \pm 0.35^{A,a}$	$43.50 \pm 0.85^{A,a}$
	Microcapsules	$44.08 \pm 0.38^{A,a}$	$43.77 \pm 0.03^{A,a}$	$44.22 \pm 0.30^{A,a}$

Table 3. Inhibition zone diameters (mm) of unencapsulated CO and encapsulated CO samples against *E. coli* and *S. aureus* at different oil concentrations (mg/well).

weaker interactions with alginate and partial relaxation or swelling of the polymeric network. This structural transition increases the permeability of the microcapsule wall, allowing the diffusion of the encapsulated CO into the surrounding medium. Additionally, the presence of ions in the simulated intestinal fluid may further promote the disintegration of the coacervate matrix by competing with polymer-polymer interactions. Although the release rate increased significantly in the intestinal phase, the cumulative release did not reach 100%, which agrees with previous reports describing the sustained and incomplete diffusion of core material from alginate-based coacervate systems under gastrointestinal conditions[70]. Comparable behavior was observed for alginate–chitosan and gelatin–acacia systems containing essential oils, where the release was significantly accelerated in the intestinal phase due to electrostatic rearrangements and polymer relaxation[71,72].

Overall, this two-phase release behavior demonstrates the pH-responsive characteristics of the FGe–SA coacervate system. The microcapsules displayed stability under gastric conditions, protecting the encapsulated oil from premature release, while exhibiting a controlled and gradual release as the pH increased. These results indicate that the encapsulated clove oil remained effectively retained in the acidic environment and was released progressively in the intestinal phase, reflecting the potential of the developed formulation to modulate the release of hydrophobic bioactives in pH-variable conditions such as those of the gastrointestinal tract.

In vitro antimicrobial effects of microcapsules

The antimicrobial activity of unencapsulated CO and its microencapsulated form against *E. coli* and *S. aureus*, expressed as inhibition zone diameters, is presented in Table 3. In general, both samples exhibited inhibitory effects on the tested bacteria, and for *E. coli*, the inhibition zones increased significantly from 2.5 to 5 mg/well ($p < 0.05$), whereas no further increase was observed between 5 and 10 mg/well. In contrast, this concentration-dependent effect was not evident for *S. aureus*. However, the extent of inhibition varied depending on the bacterial strain and sample type.

For *E. coli*, the inhibition zones produced by unencapsulated CO ranged from 37.07 ± 0.35 mm to 40.92 ± 0.95 mm, whereas those obtained from the microcapsules ranged from 37.00 ± 1.52 mm to 42.53 ± 1.16 mm. Although the difference between unencapsulated and encapsulated samples was not statistically significant at the lowest concentration, a higher inhibition was observed for the microcapsules at higher concentrations ($p < 0.05$). In previous studies, the enhanced antimicrobial activity of encapsulated essential oils was attributed to several complementary factors, including improved stability of volatile compounds, increased solubility and

dispersion in aqueous media, protection of active constituents such as thymol, carvacrol, or cinnamaldehyde from degradation, and enhanced bioavailability of these key components. These factors collectively contribute to a more sustained and effective interaction between the active molecules and bacterial cells[73,74].

The larger inhibition zones observed for *S. aureus* compared to *E. coli* can be attributed to structural differences between Gram-positive and Gram-negative bacteria. Gram-positive bacteria possess a thick peptidoglycan layer and lack an outer membrane, which facilitates the penetration of hydrophobic antimicrobial compounds such as eugenol. In contrast, the lipopolysaccharide-rich outer membrane of Gram-negative bacteria acts as an effective permeability barrier, limiting the diffusion of these molecules and thereby reducing their susceptibility[75].

The antimicrobial effect of the microcapsules was dependent on the bacterial strain. For *E. coli*, microcapsules showed higher activity at certain concentrations, which can be attributed to the controlled release and improved diffusion of clove oil from the capsule matrix. In contrast, for *S. aureus*, both microcapsules and unencapsulated oil exhibited similar antimicrobial activity, indicating that free clove oil already provides sufficient antibacterial effect against Gram-positive bacteria, thereby limiting the additional benefit of encapsulation.

The inhibition zones for *S. aureus* ranged from 42.43 ± 0.39 mm to 43.50 ± 0.85 mm for unencapsulated oil and from 44.08 ± 0.38 mm to 44.22 ± 0.30 mm for the encapsulated samples. The slightly greater zones obtained for the microcapsules suggest that encapsulation preserved the antimicrobial efficacy of CO while potentially providing a more sustained release of active compounds. These results demonstrate that the encapsulation process did not diminish the antimicrobial effectiveness of CO; on the contrary, the microcapsules maintained or slightly improved its antibacterial activity, particularly at higher concentrations against *E. coli*.

Increasing the amount of unencapsulated CO from 5 to 10 mg/well did not significantly increase the inhibition zone diameter ($p > 0.05$). A similar trend was also reported by Anaya-Castro et al., (2017), where increasing the amount of encapsulated CO beyond a certain level did not further enhance the antimicrobial effect. This behavior was attributed to supersaturation and limited release of the oil from β-cyclodextrin complexes, which restricted its diffusion into the medium[76].

Values are expressed as mean ± standard deviation ($n = 3$). Different uppercase letters in the same column and different lowercase letters in the same row indicate significant differences ($p < 0.05$).

Conclusion

In this study, FGe and SA were used to encapsulate CO through complex coacervation. The formation of coacervates was influenced by both pH and the ratio of the two biopolymers, and the interaction was mainly driven by electrostatic attraction and hydrogen bonding. By evaluating turbidity, zeta potential, and coacervate yield, suitable coacervation conditions were identified. These findings were later applied to optimize the encapsulation process using response surface methodology, which helped to achieve high encapsulation efficiency and yield. The morphological appearance and FTIR spectra confirmed the successful encapsulation of CO within the coacervate wall. The obtained microcapsules exhibited favorable physical properties, including moderate moisture content, acceptable hygroscopicity, and good solubility. Thermal analysis indicated that encapsulation improved the heat resistance of CO, suggesting better protection against thermal degradation. The antimicrobial results showed that the encapsulated CO maintained its inhibitory effect against *S. aureus* and displayed relatively higher activity against *E. coli* than the unencapsulated CO. Moreover, the microcapsules remained stable in simulated gastric conditions and released the oil gradually as the pH increased, demonstrating their potential to protect the oil during digestion. These findings indicate that the FGe–SA complex coacervation system was effective for CO encapsulation, and further studies could clarify its suitability for other types of essential oils.

Data availability

The datasets generated during and/or analysed during the current study are available from the corresponding author on reasonable request.

Received: 28 November 2025; Accepted: 17 April 2026
Published online: 21 April 2026

References

1. Bhavaniramya, S., Vishnupriya, S., Al-Aboody, M. S., Vijayakumar, R. & Baskaran, D. Role of essential oils in food safety: Antimicrobial and antioxidant applications. *Grain Oil Sci. Technol.* **2**, 49–55 (2019).
2. Diogo Gonçalves, S., Paiva-Cardoso, M. D. N. & Caramelo, A. Green preservation strategies: The role of essential oils in sustainable food preservatives. *Sustainability* **17**, 7326 (2025).
3. Maurya, A., Prasad, J., Das, S. & Dwivedy, A. K. Essential oils and their application in food safety. *Front. Sustain. Food Syst.* **5**, 653420 (2021).
4. Wang, L. et al. Preservation effects of chitosan/polyvinyl alcohol/clove essential oil antifungal film on yellow peaches: Physicochemical properties and fruit quality assessment. *Food Control*. **164**, 110582 (2024).
5. Islam, M. K. et al. A review on olive and clove: Promising natural additives for seafood preservation. *Food Humanity*. **4**, 100539 (2025).
6. Xu, P. et al. Chitosan nanocapsules encapsulating antioxidant peptides and clove oil: Characterization, antioxidant and antibacterial activities, and impact on strawberry quality. *Int. J. Biol. Macromol.* **312**, 143983 (2025).
7. Misra, S., Pandey, P. & Mishra, H. N. Novel approaches for co-encapsulation of probiotic bacteria with bioactive compounds, their health benefits and functional food product development: A review. *Trends Food Sci. Technol.* **109**, 340–351 (2021).
8. Yammine, J., Chihib, N. E., Gharsallaoui, A. & Ismail, A. Karam, L. Advances in essential oils encapsulation: development, characterization and release mechanisms. *Polym. Bull.* **81**, 3837–3882 (2024).
9. Muhoza, B. et al. Spray-and freeze-drying of microcapsules prepared by complex coacervation method: A review. *Food Hydrocoll.* **140**, 108650 (2023).

10. Costa, M. J. A. et al. Fish gelatin in biomedical applications: A systematic review. *J. Drug Deliv. Sci. Technol.* 107627 https://doi.org/10.1016/j.jddst.2025.107627 (2025).
11. Mutlu, N. Effects of grape seed oil nanoemulsion on physicochemical and antibacterial properties of gelatin–sodium alginate film blends. *Int. J. Biol. Macromol.* **237**, 124207 (2023).
12. Annappa, H., Tamatam, A., Nallamuthu, I. & Ranganathan, K. Formulation of pH-responsive nanoparticles using zein/sodium alginate polymers for enhanced bioavailability of the vitamin D3. *Int. J. Biol. Macromol.* **313**, 144140 (2025).
13. Cui, Y., Chen, K., Chen, K., Li, Y. & Jiang, L. The complex coacervation of gum Arabic and krill protein isolate and their application for Antarctic krill oil encapsulation. *Carbohydr. Polym.* **348**, 122831 (2025).
14. Chen, X. et al. Gelatin/peach gum complex coacervated microcapsules loaded with cinnamon essential oil: Preparation, characterization, antibacterial properties and its application in mushroom (*Agaricus bisporus*). *Food Control.* **171**, 111129 (2025).
15. Ma, D., Yang, B., Zhao, J., Yuan, D. & Li, Q. Advances in protein-based microcapsules and their applications: A review. *Int. J. Biol. Macromol.* **263**, 129742 (2024).
16. Plati, F. & Paraskevopoulou, A. Hemp protein isolate – gum Arabic complex coacervates as a means for oregano essential oil encapsulation. Comparison with whey protein isolate – gum Arabic system. *Food Hydrocoll.* **136**, 108284 (2023).
17. Djihad, N. et al. Microencapsulation of Citrus limon essential oil by complex coacervation and release behavior of terpenic and derived volatile compounds. *Food Hydrocoll.* **152**, 109830 (2024).
18. Zhang, L., Zhang, M., Ju, R., Bhandari, B. & Liu, K. Antibacterial mechanisms of star anise essential oil microcapsules encapsulated by rice protein-depolymerized pectin electrostatic complexation and its application in crab meatballs. *Int. J. Food Microbiol.* **384**, 109963 (2023).
19. Liu, Z. et al. Preparation of *Cinnamomum camphora* essential oil microcapsules using gelatin/gum arabic and evaluation of their antifungal effects on Fusarium spp. *Int. J. Biol. Macromol.* **303**, 140706 (2025).
20. Daza, L. D., López, S. D., Montealegre, M. Á. & Eim, V. S. Sandoval-Aldana, A. Study of the physicochemical properties of hass avocado oil encapsulated by complex coacervation. *LWT Food Sci. Technol.* **204**, 116491 (2024).
21. Chen, Q., Zhao, C., Ma, X., Yan, W. & Wang, F. Preparation and characterization of walnut oil microcapsules by complex coacervation with sodium alginate and chitosan. *LWT Food Sci. Technol.* **222**, 117630 (2025).
22. Mu, J., Hu, R., Tang, Y., Dong, W. & Zhang, Z. Microencapsulation of green coffee oil by complex coacervation of soy protein isolate, sodium casinate and polysaccharides: Physicochemical properties, structural characterisation, and oxidation stability. *Int. J. Biol. Macromol.* **256**, 128064 (2024).
23. Hosseini, S. F., Zandi, M., Rezaei, M. & Farahmandghavi, F. Two-step method for encapsulation of oregano essential oil in chitosan nanoparticles: Preparation, characterization and in vitro release study. *Carbohydr. Polym.* **95**, 50–56 (2013).
24. Zhou, Y. et al. Ultrasound-assisted, machine learning-optimized extraction of silver carp viscera fish oil and microencapsulation via complex coacervation. *Ultrason. Sonochem.* **120**, 107452 (2025).
25. Kolotova, D. S. et al. Phase behavior of aqueous mixtures of sodium alginate with fish gelatin: Effects of pH and ionic strength. *Polymers* **15**, 2253 (2023).
26. Brahmi, M., Essifi, K., Elbachiri, A. & Tahani, A. Adsorption of sodium alginate onto sodium montmorillonite. *Mater. Today Proc.* **45**, 7789–7793 (2021).
27. Su, C. R. et al. A novel complex coacervate formed by gliadin and sodium alginate: Relationship to encapsulation and controlled release properties. *LWT Food Sci. Technol.* **139**, 110591 (2021).
28. Li, F., Wang, H. & Mei, X. Preparation and characterization of phytosterol-loaded microcapsules based on the complex coacervation. *J. Food Eng.* **311**, 110728 (2021).
29. Li, L. et al. Characterization of complex coacervation between chia seed gum and whey protein isolate: Effect of pH, protein/polysaccharide mass ratio and ionic strength. *Food Hydrocoll.* **148**, 109445 (2024).
30. Derkach, S. R., Kolotova, D. S., Voron'ko, N. G., Obluchinskaya, E. D. & Malkin, A. Ya. Rheological properties of fish gelatin modified with sodium alginate. *Polymers* **13**, 743 (2021).
31. He, L. et al. Microencapsulation of *Angelica sinensis* essential oil by complex coacervation using chitosan and gelatin: Optimization, characterization, in vitro digestion, and biological activity. *Int. J. Biol. Macromol.* **316**, 144365 (2025).
32. Lan, Y., Ohm, J. B., Chen, B. & Rao, J. Microencapsulation of hemp seed oil by pea protein isolate–sugar beet pectin complex coacervation: Influence of coacervation pH and wall/core ratio. *Food Hydrocoll.* **113**, 106423 (2021).
33. Kaushik, P., Dowling, K., McKnight, S., Barrow, C. J. & Adhikari, B. Microencapsulation of flaxseed oil in flaxseed protein and flaxseed gum complex coacervates. *Food Res. Int.* **86**, 1–8 (2016).
34. Eghbal, N. & Choudhary, R. Complex coacervation: Encapsulation and controlled release of active agents in food systems. *LWT Food Sci. Technol.* **90**, 254–264 (2018).
35. Mehrnia, M. A., Jafari, S. M., Makhmal-Zadeh, B. S. & Maghsoudlou, Y. Rheological and release properties of double nano-emulsions containing crocin prepared with Angum gum, Arabic gum and whey protein. *Food Hydrocoll.* **66**, 259–267 (2017).
36. Liu, J., Shim, Y. Y., Shen, J., Wang, Y. & Reaney, M. J. Whey protein isolate and flaxseed (*Linum usitatissimum* L.) gum electrostatic coacervates: Turbidity and rheology. *Food Hydrocoll.* **64**, 18–27 (2017).
37. Zhou, X., Feng, X., Qi, W., Zhang, J. & Chen, L. Microencapsulation of vitamin E by gelatin-high/low methoxy pectin complex coacervates: Effect of pH, pectin type, and protein/polysaccharide ratio. *Food Hydrocoll.* **151**, 109794 (2024).
38. Barresi, A. A. et al. Monitoring of the primary drying of a lyophilization process in vials. *Chem. Eng. Process Process. Intensif.* **48**, 408–423 (2009).
39. Mohseni, F. & Goli, S. A. H. Encapsulation of flaxseed oil in the tertiary conjugate of oxidized tannic acid-gelatin and flaxseed (*Linum usitatissimum*) mucilage. *Int. J. Biol. Macromol.* **140**, 959–964 (2019).
40. Tavares, L. & Noreña, C. P. Z. Encapsulation of ginger essential oil using complex coacervation method: Coacervate formation, rheological property, and physicochemical characterization. *Food Bioprocess. Technol.* **13**, 1405–1420 (2020).
41. Koupantsis, T., Pavlidou, E. & Paraskevopoulou, A. Flavour encapsulation in milk proteins–CMC coacervate-type complexes. *Food Hydrocoll.* **37**, 134–142 (2014).
42. Huang, J. et al. Preparation and characterization of resveratrol-loaded microcapsules with whey protein and flaxseed gum by membrane emulsification and complex coacervation methods. *Int. J. Biol. Macromol.* **306**, 141783 (2025).
43. Zhu, J. et al. Preparation of spray-dried soybean oil body microcapsules using maltodextrin: Effects of dextrose equivalence. *LWT Food Sci. Technol.* **154**, 112874 (2022).
44. Bakry, A. M., Huang, J., Zhai, Y. & Huang, Q. Myofibrillar protein with κ- or λ-carrageenans as novel shell materials for microencapsulation of tuna oil through complex coacervation. *Food Hydrocoll.* **96**, 43–53 (2019).
45. Ng, L. H., Ling, J. K. U. & Hadinoto, K. Formulation strategies to improve the stability and handling of oral solid dosage forms of highly hygroscopic pharmaceuticals and nutraceuticals. *Pharmaceutics.* **14**, 2015 (2022).
46. Tavares, L. & Noreña, C. P. Z. Encapsulation of garlic extract using complex coacervation with whey protein isolate and chitosan as wall materials followed by spray drying. *Food Hydrocoll.* **89**, 360–369 (2019).
47. Nurhad, B., Andoyo, R. & Indiarto, R. Study the properties of honey powder produced from spray drying and vacuum drying method. *Int. Food Res. J.* **19**, 907 (2012).
48. Pellicer, J. A. et al. Stability of microencapsulated strawberry flavour by spray drying, freeze drying and fluid bed. *Powder Technol.* **347**, 179–185 (2019).
49. Wang, L. et al. Study on preparation and properties of *Camellia oleifera* seed oil microcapsules by complex coacervation and spray drying. *LWT - Food Sci. Technol.* **184**, 115056 (2023).

50. Zhang, W. et al. Complex coacervation of low methoxy pectin with three types of gelatins for the encapsulation of fish oil. *Food Chem.* **460**, 140567 (2024).
51. Klinkesorn, U., Sophanodora, P., Chinachoti, P., Decker, E. A. & McClements, D. J. Characterization of spray-dried tuna oil emulsified in two-layered interfacial membranes prepared using electrostatic layer-by-layer deposition. *Food Res. Int.* **39**, 449–457 (2006).
52. Tontul, I. & Topuz, A. Spray-drying of fruit and vegetable juices: Effect of drying conditions on the product yield and physical properties. *Trends Food Sci. Technol.* **63**, 91–102 (2017).
53. Hashim, S. B. H. et al. Fabrication of biopolymer stabilized microcapsules for enhancing physicochemical stability, antioxidant and antimicrobial properties of cinnamon essential oil. *Int. J. Biol. Macromol.* **271**, 132336 (2024).
54. Rodríguez-Cortina, A. & Hernández-Carrión, M. Microcapsules of Sacha Inchi seed oil (*Plukenetia volubilis* L.) obtained by spray drying as a potential ingredient to formulate functional foods. *Food Res. Int.* **170**, 113014 (2023).
55. Fernandes, G. D. J. C. et al. Effect of polyvinyl alcohol and carboxymethylcellulose on the technological properties of fish gelatin films. *Sci. Rep.* **12**, 10497 (2022).
56. Liu, C. et al. The impacts of different modification techniques on the gel properties and structural characteristics of fish gelatin. *Food Hydrocoll.* **158**, 110536 (2025).
57. Diana, M. I., Selvin, P. C., Selvasekarapandian, S. & Krishna, M. V. Investigations on Na-ion conducting electrolyte based on sodium alginate biopolymer for all-solid-state sodium-ion batteries. *J. Solid State Electrochem.* **25**, 2009–2020 (2021).
58. Cui, P. et al. Preparation and properties of walnut oil microcapsules. *LWT Food Sci. Technol.* **225**, 117853 (2025).
59. Miranda, C. S., Antunes, J. C., Homem, N. C. & Felgueiras, H. P. Controlled release of cinnamon leaf oil from chitosan microcapsules embedded within a sodium alginate/gelatin hydrogel-like film for Pseudomonas aeruginosa Elimination. *Proc* **69**, 39 (2020).
60. Jeong, S., Kim, B., Lau, H. C. & Kim, A. Gelatin-alginate complexes for EGF encapsulation: Effects of h-bonding and electrostatic interactions. *Pharm* **11**, 530 (2019).
61. de López, C., Settier-Ramírez, L., Gavara, R. & Hernández-Muñoz, P. López Carballo, G. Development of biodegradable films loaded with phages with antilisterial properties. *Polymers* **13**, 327 (2021).
62. Tongnuanchan, P., Benjakul, S. & Prodpran, T. Structural, morphological and thermal behaviour characterisations of fish gelatin film incorporated with basil and citronella essential oils as affected by surfactants. *Food Hydrocoll.* **41**, 33–43 (2014).
63. Zhou, D. et al. Preparation of walnut oil microcapsules employing soybean protein isolate and maltodextrin with enhanced oxidation stability of walnut oil. *LWT Food Sci. Technol.* **83**, 292–297 (2017).
64. Shen, J., Zhang, M. & Yang, C. Microencapsulation of ginger essential oil using mung bean protein isolate-chitosan complex coacervates: Application in the preservation of crab meatballs and the prediction of shelf life. *Food Chem.* **449**, 139263 (2024).
65. Bajac, J. et al. Microencapsulation of juniper berry essential oil (*Juniperus communis* L.) by spray drying: Microcapsule characterization and release kinetics of the oil. *Food Hydrocoll.* **125**, 107430 (2022).
66. Wang, Y. et al. Dual cross-linking with tannic acid and transglutaminase improves microcapsule stability and encapsulates lemon essential oil for food preservation. *Food Chem.* **465**, 142173 (2025).
67. Thuekeaw, S., Angkanaporn, K., Chirachanchai, S. & Nuengjamnong, C. Dual pH responsive via double—layered microencapsulation for controlled release of active ingredients in simulated gastrointestinal tract: A model case of chitosan-alginate microcapsules containing basil oil (*Ocimum basilicum* Linn). *Polym. Degrad. Stab.* **191**, 109660 (2021).
68. Cortez-Trejo, M. C., Wall-Medrano, A., Gaytán-Martínez, M. & Mendoza, S. Microencapsulation of pomegranate seed oil using a succinylated taro starch: Characterization and bioaccessibility study. *Food Biosci.* **41**, 100929 (2021).
69. He, H. et al. Improved stability and controlled release of CLA with spray-dried microcapsules of OSA-modified starch and xanthan gum. *Carbohydr. Polym.* **147**, 243–250 (2016).
70. Azad, A. K. et al. Encapsulation of black seed oil in alginate beads as a ph-sensitive carrier for intestine-targeted drug delivery: In vitro, in vivo and ex vivo study. *Pharm* **12**, 219 (2020).
71. Plati, F., Ritzoulis, C., Pavlidou, E. & Paraskevopoulou, A. Complex coacervate formation between hemp protein isolate and gum Arabic: Formulation and characterization. *Int. J. Biol. Macromol.* **182**, 144–153 (2021).
72. Zhao, Q., Gao, Y. S., Jin, F. & Zhu, L. Y. Preparation process optimization and performance characterization of feed plant essential oil microcapsules. *Molecules* **27**, 7096 (2022).
73. Arana-Sánchez, A. et al. Antimicrobial and antioxidant activities of Mexican oregano essential oils (*Lippia graveolens* HBK) with different composition when microencapsulated in β-cyclodextrin. *Lett. Appl. Microbiol.* **50**, 585–590 (2010).
74. Cui, H., Li, W., Li, C., Vittayapadung, S. & Lin, L. Liposome containing cinnamon oil with antibacterial activity against methicillin-resistant *Staphylococcus aureus* biofilm. *Biofouling* **32**, 215–225 (2016).
75. Akpınar, S. & Mutlu, N. Multidimensional analysis of honey from Eastern Anatolia (Kars): Pollen spectrum, physicochemical properties, and antimicrobial activity. *PLoS One*. **20**, e0327861 (2025).
76. Anaya-Castro, M. A. et al. β-Cyclodextrin inclusion complexes containing clove (Eugenia caryophyllata) and Mexican oregano (Lippia berlandieri) essential oils: Preparation, physicochemical and antimicrobial characterization. *Food Packag. Shelf.* **14**, 96–101 (2017).

Acknowledgements

This study was funded by the Scientific Research Projects Coordination Unit of Kafkas University (Grant No. 2025-FM-12). We would like to thank the staff of Bursa Technical University Central Research Laboratory (BTÜ-MERLAB) and the Eastern Anatolia High Technology Application and Research Center (DAYTAM) for their technical assistance with the analyses. We also thank Dr. Hüseyin Ertap for his assistance in graphic design.

Author contributions

E.K.: Supervision, project administration, funding acquisition, conceptualization. N.M.: Conceptualization, investigation, methodology, visualization, data curation, writing-original draft, writing-review and editing. E.K.: Data curation, investigation, methodology, validation, formal analysis, resources.

Funding

Scientific Research Projects Coordination Unit of Kafkas University (Grant No. 2025-FM-12).

Declarations

Competing interests

The authors declare no competing interests.

Declaration of generative AI and AI-assisted technologies in the manuscript preparation process

During the preparation of this work, the authors used ChatGPT (OpenAI) to assist with English translation and language editing. After using this tool, the authors carefully reviewed and revised the text to ensure accuracy and takes full responsibility for the final content.

Additional information

Correspondence and requests for materials should be addressed to N.M.

Reprints and permissions information is available at www.nature.com/reprints.

Publisher's note Springer Nature remains neutral with regard to jurisdictional claims in published maps and institutional affiliations.

Open Access This article is licensed under a Creative Commons Attribution-NonCommercial-NoDerivatives 4.0 International License, which permits any non-commercial use, sharing, distribution and reproduction in any medium or format, as long as you give appropriate credit to the original author(s) and the source, provide a link to the Creative Commons licence, and indicate if you modified the licensed material. You do not have permission under this licence to share adapted material derived from this article or parts of it. The images or other third party material in this article are included in the article's Creative Commons licence, unless indicated otherwise in a credit line to the material. If material is not included in the article's Creative Commons licence and your intended use is not permitted by statutory regulation or exceeds the permitted use, you will need to obtain permission directly from the copyright holder. To view a copy of this licence, visit http://creativecommons.org/licenses/by-nc-nd/4.0/.

© The Author(s) 2026